DISSERTATION

Towards fast He beam edge plasma diagnostics

ausgeführt zum Zwecke der Erlangung des akademischen Grades eines

Doktors der technischen Wissenschaften

unter der Leitung von

o. Univ.-Prof. HP. Winter

E134

Institut für Allgemeine Physik

eingereicht an der Technischen Universität Wien

Technisch-Naturwissenschaftliche Fakultät

von

Dipl.-Ing. Michael PROSCHEK

Matr.-Nr. 9025445

Bräuhausgasse 11/15

A-1050 WIEN

Wien, am 21. Dezember 2001

Kurzfassung

Die genaue Kenntnis der Randschichteigenschaften ist für die Entwicklung von Hochtemperaturplasmen mit reaktorrelevanten Parametern von entscheidender Bedeutung. Dabei werden hohe Anforderungen bezüglich räumlicher und zeitlicher Auflösung gestellt, um steile Dichteprofile von H-mode-Plasmen und sogenannten „Advanced Scenarios“ räumlich auflösen zu können. Eine gute Zeitauflösung ist notwendig, um Instabilitäten in der Randschicht („ELMs“) und Fluktuationen untersuchen zu können. Aktive Spektroskopie mit injizierten Atomstrahlen hat sich in vielen Bereichen der Plasmadiagnostik als fundamentale Untersuchungsmethode für mehrere Plasmaparameter etabliert. In der vorliegenden Dissertation wird die Entwicklung einer aktiven Strahlemissionsdiagnostik mit einem schnellen neutralen He-Strahl beschrieben und deren Eignung als Dichte- und Temperaturdiagnostik untersucht.

Der zentrale Teil der Arbeit beschäftigt sich mit orientierenden Messungen, die an zwei der führenden Fusionsexperimente (ASDEX-Upgrade in Garching/DE und JET in Culham/UK) durchgeführt wurden. Zur Erzeugung der schnellen He-Strahlen wurden dabei Injektoren der Neutralteilchenheizung verwendet um reine He Strahlen oder He dotierte D-Strahlen zu erzeugen. Die Strahlemission der schnellen He-Atome wurde mit Hilfe der Ladungsaustausch- Spektrometer des jeweiligen Experiments gemessen.

Mehrere HeI-Singulett- und Triplett-Linien ausreichender Intensität konnten im sichtbaren Bereich gemessen werden, wobei die Empfindlichkeit der verwendeten Spektrometer gegen beide Enden des sichtbaren Bereichs hin diskriminiert war. Die Doppler-verschobene Strahlemission ist als reine Linienstrahlung in der Regel ungestört von Verunreinigungsemissionen gut meß- und auswertbar. Die Emission von Triplettlinien ist auf die äußeren 200 mm des Plasmas beschränkt, jene von Singulettlinien hingegen über den gesamten beobachteten Bereich meßbar, jedoch am Maximum um eine Größenordnung schwächer als die höchste Intensität der stärksten Triplettlinie. Aus der Form der Singulett-Emissionsprofile konnte auch der anfängliche Anteil an metastabilen 2^1S Atomen im He-Strahl bestimmt werden.

Emissionprofile der intensivsten HeI-Singulettlinie (2^1P-3^1D) bei 667.8 nm und der intensivsten Triplettlinie (2^3P-3^3D) bei 587.6 nm wurden an AUG für unterschiedliche Plasmaentladungen gemessen. Außerdem konnte die Streuung der Messergebnisse anhand einer Messreihe an nahezu identischen Plasmaentladungen bestimmt werden.

Bei JET wurden Emissionsprofile mit guter räumlicher Auflösung bestimmt. Diese hohe Auflösung konnte dadurch erreicht werden, dass das Plasma während der Messung quer zu den Sichtlinien verschoben wurde. Neben dieser erhöhten Auflösung erlaubte diese neue Experimentiertechnik auch benachbarte Kanäle des Spektrometers relativ zueinander zu kalibrieren, was zu einer deutlichen Reduzierung der Messfehler führte. Eine weitere interessante Beobachtung ist, dass die Form der Triplett-Emissionsprofile auch von der Verteilung der Plasmaverunreinigungen beeinflusst wird. Dies öffnet die Möglichkeit zur Entwicklung einer Z_{eff}-Diagnostik.

Die Emissionsprofile werden mit einem numerischen Stoß-Strahlungsmodell simuliert und mit den Messungen verglichen. Das Modell wurde im Rahmen dieser Arbeit erweitert und bezüglich Rechenzeit optimiert. Das eigentliche Ziel der vorliegenden Arbeit war es, Dichte- und Temperaturprofile aus den gemessenen Emissionsprofilen ableiten zu können. Dazu wurde der Umkehrcode `yttocs` entwickelt. Dieser beruht auf einer Variationsmethode, in der die Modellrechnungen oftmals aufgerufen werden, was u.a. die Entwicklung einer geschwindigkeits-optimierten Subroutine notwendig machte.

Die ersten Tests dieses Umkehrcodes wurden mit synthetischen Daten vorgenommen um etwaige Fehler in der Aufbereitung der atomaren Daten zu vermeiden. Der Code zeigt gutes Konvergenzverhalten; sowohl Dichte- als auch Temperaturprofile konnten aus den Emissionsprofilen zweier unterschiedlicher Heliumlinien extrahiert werden. Damit konnte gezeigt werden, dass schnelle He-Strahlen für Elektronendichte- und -temperaturdiagnostik geeignet sind, und darüber hinaus auch für die Bestimmung anderer Plasmaparameter anwendbar sein könnten.

Abstract

A precise knowledge of the plasma edge parameters is essential for the development of reactor relevant plasmas. High spatial and temporal resolution is required in order to resolve the steep profiles of H-mode plasmas in so-called “advanced scenarios”. A good temporal resolution is advantageous for investigating edge instabilities (ELMs) and fluctuations. Active spectroscopy of injected atomic beams is a well established diagnostics for a wide range of plasma parameters. In this thesis the development of an active beam emission diagnostics with fast neutral He beams is described and its applicability as density- and temperature diagnostic investigated.

This thesis mainly deals with proof-of-principle measurements performed at two of the leading fusion experiments (ASDEX upgrade in Garching / GE and JET in Culham / UK). For generation of fast He beams the injectors of the neutral particle heating system have been used to produce either pure He beams or He doped D-beams. For observation of the He beam emission the charge-exchange-spectroscopic systems have been used at both experiments.

Several HeI singlet- and triplet lines with sufficient intensity could be identified in the visible range. However, on either end of the visible range the sensitivity of the spectrometer was too low. The HeI beam emission appears in the spectrum as a clean Doppler-shifted peak, largely undisturbed by impurity emission. Emission from the triplet levels is limited to the outer 200 mm of the plasma. The singlet emission could be detected over the full observation range, but its maximum is about one order of magnitude lower then the maximum of the most intense triplet emission. The initial metastable 2^1S fraction of the beam could be derived from the shape of the singlet HeI beam emission profile.

Emission profiles of the most intense HeI singlet line (2^1P-3^1D) at 667.8 nm and the most intense triplet line (2^3P-3^3D) at 587.6 nm could be measured at AUG for different plasma discharges. Furthermore, repetitive measurements of nominally identical pulses allowed to estimate the scatter in the data.

At JET, measurements of emission profiles with good spatial resolution could be achieved by sweeping the plasma across the viewing lines during the measurement. Besides the higher resolution this experimental technique also made it possible to cross-calibrate neighbouring channels, which yielded significantly reduced measurement errors.

Another interesting observation is the influence of the plasma impurity distribution on the triplet beam emission profile, giving the prospect for a new Z_{eff} diagnostics.

The measured emission profiles have been compared with calculations from a numerical collisional-radiative model. This model has been extended and optimised in performance as part of this thesis. The main goal of this work was to derive the electron density- and -temperature profiles from the measured HeI emission profiles. The developed reversion code is based on a variational method, which calls the model calculation-code many times and therefore required a subroutine which was optimised with respect to speed.

For the first tests with the reversion code, synthetic data were generated in order to overcome possible errors in the look-up tables generated from the atomic data. The code shows good convergence, and both electron density and -temperature could be derived from sets of two different HeI emission profiles. In summary, the results show convincingly that fast He beam emission spectroscopy can be used as an electron density- and-temperature diagnostics particularly for the plasma edge. Furthermore, there is also the prospect for other diagnostic applications.

Contents

In this corner of the following pages you will find a "flip-book" showing the flux-surfaces of the JET discharge JPN 52799. (printed version only!) Please pay attention to the plasma sweep at the end of the discharge.

1 Introduction

1.1 Motivation

The development of novel diagnostic tools providing reliable quantitative values for plasma parameters has been a key factor in the progress of fusion research towards break-even conditions. Of special importance in this area has been the use of neutral beams for active charge exchange spectroscopy which has led to a revolution of spectroscopic techniques [1].

Charge exchange recombination spectroscopy (CXRS) makes use of the emission of radiation following electron capture by fully stripped plasma ions from neutral beam particles. Low Z impurity density and temperature can be deduced from the intensity and width of the emitted line while the impurity flow velocity (plasma rotation) is obtained from the Doppler shift [2, 3, 4, 5, 6]. Beam emission spectroscopy (BES) is used to measure plasma density fluctuations [7, 8, 9, 10], the local pitch angle of the magnetic field is determined from the polarisation of the Stark or Zeemann emission and the total magnetic field strength from the wavelength splitting of multiplets [11, 12, 13, 14]. Another application based on the injection of fast neutral particles is the measurement of the plasma density through Rutherford scattering of these fast beam particles [15, 16, 17]. Several experiments make use of dedicated diagnostic beam lines, frequently operating with helium [18, 19, 20, 21, 22]. Helium beams offer several advantages over hydrogen beams: deeper penetration, the option of diagnosing alpha particles via resonant charge exchange [23, 24] and reduced intensity of background radiation from the scrape-off layer which can mask the measurements.

Optical emission from energetic lithium beams [25] has been successfully used as a diagnostic of plasma density. Due to the low ionisation energy of only 5.4 eV the excitation rate coefficient of lithium quickly looses its electron energy dependence with increasing electron energy. This, being beneficial for a pure density diagnostics, makes lithium unsuitable as a temperature diagnostics. Helium with its much higher ionisation energy of 24.6 eV has some potential for simultaneous density- and temperature diagnostics for the plasma edge. This has been verified with thermal helium beams [26]. Both diagnostics – fast lithium beams and thermal helium beams – are limited in range by the penetration depth of the neutral particles to the outer regions of the plasma. Energetic helium atoms penetrate much deeper into the plasma than either lithium atoms of similar energy or thermal helium atoms, and therefore offer the prospect for measuring TOKAMAK plasma parameters inside of the H-mode- and even internal transport barriers (ITB).

Helium as an atom with two electrons has two different spin systems, the singlet system (i. e. the spins of the two electrons are antiparallel: $S = \Sigma s_i = 0$) and the triplet system (i. e. the spins of the two electrons are parallel: $S = \Sigma s_i = 1$). The triplet system can only be populated by spin-changing processes from the ground state, i.e. electron collisions, whereas the singlet levels are mainly populated by spin-conserving processes from the ground state. The different behaviour of cross-sections for spin-conserving and spin-changing collisions leads to a rather different temperature dependence of the excitation rate coefficients even for electron

energies of some 10 keV, which are typical for the plasma core. Fig. 1.1 shows the temperature dependence of some rate coefficients for impact excitation from the ground state (2^1S) and from the triplet metastable state (2^3S).

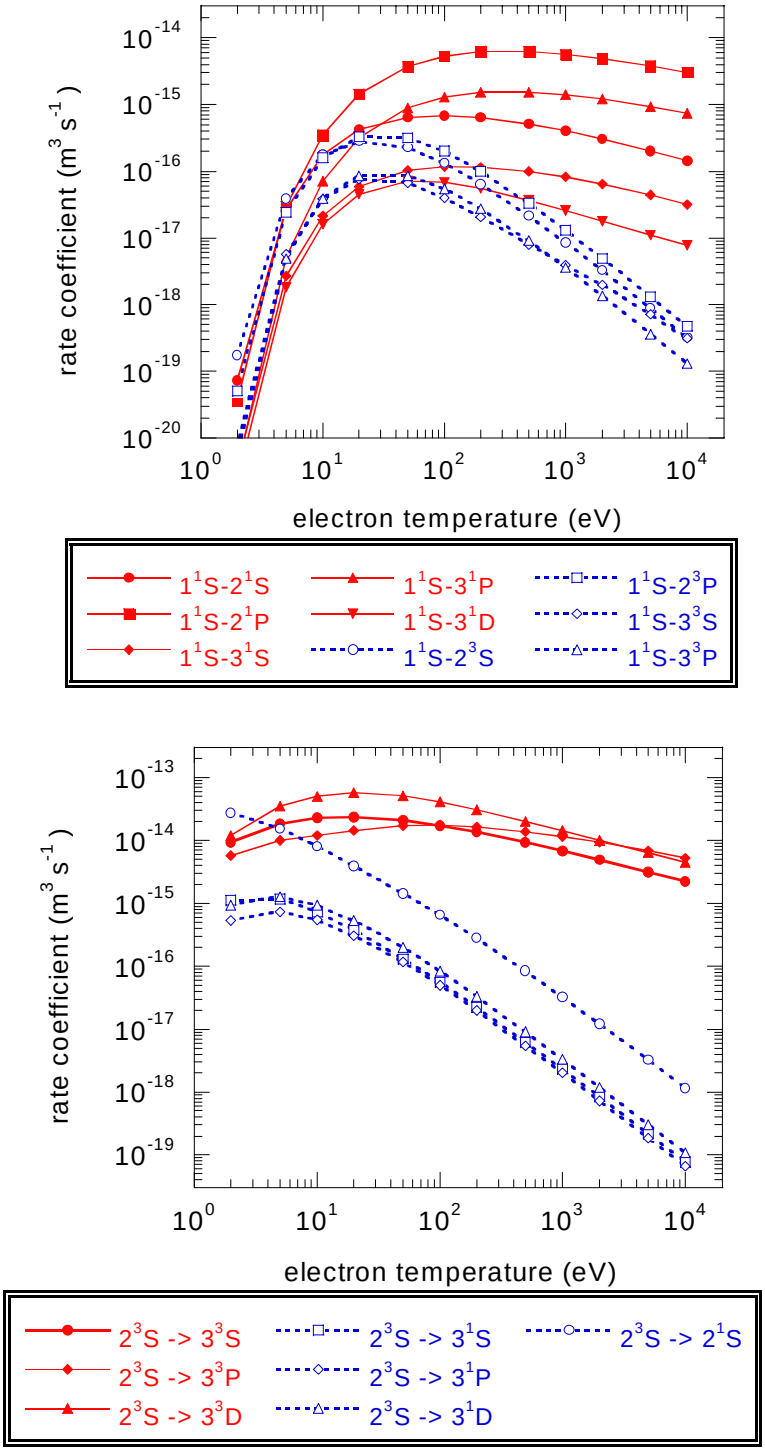

Fig. 1.1: Electron temperature dependence of rate coefficients for electron impact excitation out of the He ground state (1^1S) into several excited levels.

1.2 Beam emission spectroscopy

The passive visible spectroscopy of the plasma is limited to its edge, as essentially all atoms are fully stripped inside a hot fusion plasma. By injecting fast neutral particles a wide range of parameters becomes accessible to active spectroscopy. Most of the major fusion devices have to make use of neutral beam heating systems for active spectroscopy, since dedicated diagnostic beams are only available in a few experiments. The emission of the beam particles (D_α) are analysed by the so-called beam emission spectroscopy (BES), however due to the complexity of the spectrum it is not being used as a standard diagnostic for plasma density [27]. Both JET and AUG use a fast Li-beam for deduction of the edge density profile via impact excitation spectroscopy (Li-IXS). No fast H/D-diagnostic beam is installed on either experiment for spectroscopic measurements. However, dedicated beam sources of the heating beam systems are routinely used for CXRS and MSE.

As shown in chapter 2.2, the HeI beam emission spectrum is much simpler than the beam emission spectrum of hydrogen and therefore offers the prospect for density- and temperature diagnostics. This has so far not been possible for routine operation, as the production of helium beams requires a specialised helium pumping capacity which is not available during normal operation. This problem has been overcome by using a so called doped beam [28]. In this mode of beam operation a small quantity of helium gas is additionally injected into the beam source operating with hydrogen or deuterium. The injection of helium is restricted to time periods during which the fast helium atoms are required. This and the fact that the hydrogen gas in the neutraliser is used for neutralisation of the helium ions allows to reduce the helium gas flow to a level at which no additional helium pumping capacity is required. Such doped beams can therefore be made available without adverse effects on the availability of the neutral beam heating system.

Using the heating beams for beam emission spectroscopy limits the spatial resolution of the measurement, as these heating beams have a diameter of typically 150 – 300 mm. This is a severe restriction for diagnosing the narrow edge region. Another potential disadvantage of using the powerful heating beam is that the latter might strongly influence the local plasma parameters. Both these problems could be overcome with a dedicated diagnostic beam. However, for the proof-of-principle experiments described in this paper only the heating beams were available.

1.3 Collisional-radiative model for calculation of beam emission profiles

The model used in this paper has been described in detail in the Ph.D. thesis of S. Menhart [29] and can be summarised as follows:

The level population of fast He beam particles interacting with a plasma of given density- and temperature distribution is calculated stepwise, starting with a given initial population.

In order to calculate the change in the population of the HeI levels within a step *dx* along the beam we have to solve the statistical balance equations which represent the rates at which the excited levels of an atom are populated and depopulated. In general, these equations have the shape

$$\frac{dN_i}{dt} + v_b \frac{dN_i}{dx} = \sum_{j \neq i} \langle \sigma v \rangle_{ji,population} n_{target} N_j - \sum_{j \neq i} \langle \sigma v \rangle_{ji,depop.} n_{target} N_j + \sum_{j,j>i} A_{ij} N_j - \sum_{j,j<i} A_{ji} N_i \qquad (1)$$

N_i and N_j denote the population densities of level *i* and *j*, respectively, v_b the velocity of beam particles, $<\sigma v>$ the rate coefficient of the collisional processes, n_{target} the density of the target (in this case plasma electrons or protons), and A_{ij} the spontaneous emission coefficients for the emission from levels *j* to levels *i*.

All excitation-, de-excitation- and loss processes can be included into one matrix for a given set of parameters (n_e, T_e, E_b, Z_{eff}). The coefficients of this collisional radiative matrix M_{ij} are called 'generalised collisional radiative coefficients' (GRCs).

ADAS 311 calculates this GRCs up to high level numbers, including cross-sections from the ADAS data base and numerical approximations [30]. The ADAS code subsequently merges this big matrix into a more convenient 3x3 matrix for the transitions between the He ground state and the two metastable levels ($2s^1S$ and $2s^3S$ in Fig. 1.2) which covers the influence from the excited levels. This code provides the matrices in the n_e,v_b-plane, which is not suitable for beam emission spectroscopy with a fixed beam velocity v_b but variable plasma temperatures T_e.

We used a different version of the ADAS 311 code (not released), which is able to merge the GRCs into an arbitrary matrix size ($n_s \times n_s$) and presents the matrices in the n_e,T_e-plane. The "condensed" GRCs contain projections of all transitions from levels with $n > n_s$ which means that these levels are treated as being in equilibrium with the levels up to n_s.

So far this modified ADAS 311 code constructed by H. Anderson [31], can not be run at TU Vienna, due to incompatibilities between the sun UNIX used at Strathclyde and the LINUX system used at TU Vienna. The lookup tables (`ASCII`-files) were generated by S. Loch in Strathclyde and subsequently transferred to the LINUX computer at TU Vienna.

For a certain beam energy (E_b) the GRCs are stored in lookup-tables for a list of electron temperatures (T_e) and -densities (n_e) covering the parameter range of the plasma that is going to be analysed. The stepwise calculation of the populations by using the GRCs (matrix M_{ij}) is given in Equation 2.

$$N_i(x+dx) = N_i(x) + M_{ij}(E_b, n_e, T_e) \cdot N_j(x) \cdot \frac{n_e(x)}{v_b} dx \qquad (2)$$

N_i and N_j denote the population densities of levels i and j, respectively and n_e the electron density at the position x. The step-width dx necessary to obtain a numerical stable solution is typically 0.1 mm for $n_s = 3$ (11x11 matrices). For increasing n_s and higher velocities v_b of the beam the step width has to be reduced.

From each location along the beam axis, the matrices with the next higher and lower density and temperature are located and the relevant GRC is created by logarithmic interpolation in the case of density and by linear interpolation in the case of temperature. The typical size of the `ASCII`-files generated by ADAS 311 is, depending on the matrix size, 1 to 10 Mbytes. It contains approximately 500 matrices, linearly spaced on a logarithmic scale.

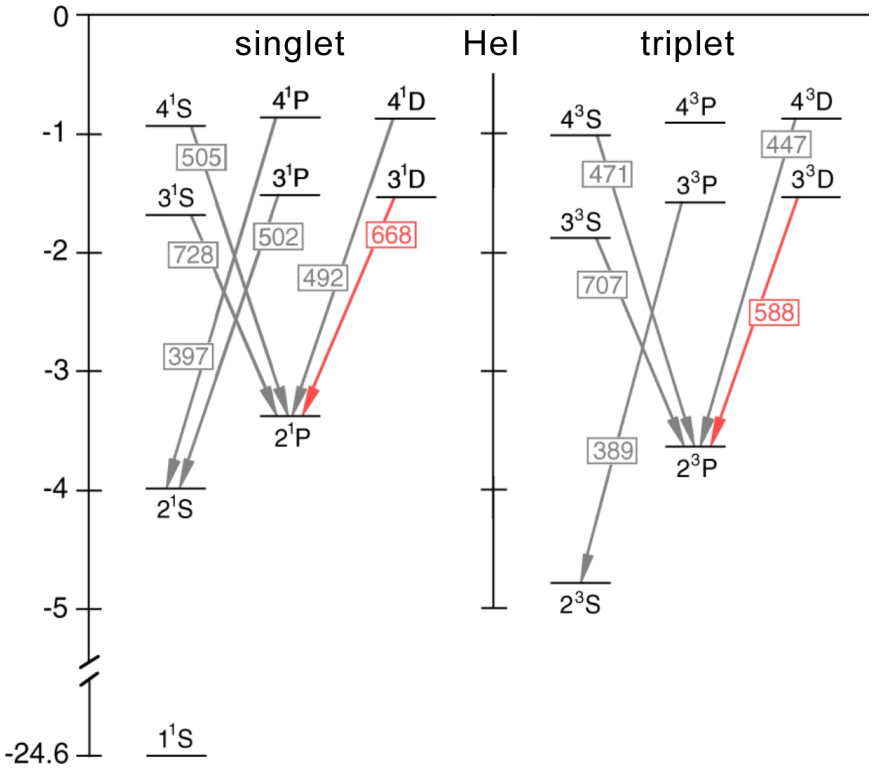

Fig. 1.2: Level diagram of HeI states with quantum numbers n<5 and related photon emission in the visible range.

The "original" `scotty` code [32] used for the modelling of the beam emission in the work of S. Menhart [29] involved a model treating the ground and metastable states as mutually independent. This simplified model becomes less well applicable with increasing beam energy. The code solving equ. 2 has therefore been rewritten in IDL (`scotty_idl`) to extend the number of independent states to a principal quantum number n_s, where n_s can be freely selected.

2 HeI beam emission measurements on medium-size and large fusion experiments

2.1 Helium doping system for heating beams

Due to the lack of dedicated fast diagnostic beams at AUG and JET the D-heating beam injectors were utilised in both cases to generate fast He beams.

Operating a neutral beam injector with He gas leads to an increase of the pressure in the beam box, because He is not pumped by the ion-getter or standard cryo pumps used in the beam injectors in order to pump the gas outflow from the neutralisers. The pressure rise causes an accordingly higher power load of the beam duct and must therefore be limited.

At JET it was possible to convert a beam box to pure He beam operation. This requires to cover the cryo pump with an argon layer before each pulse, which is time-consuming and also reduces the reliability of the system. Furthermore, under normal operating conditions the influx of He into the plasma is unwanted and operation of the beam injector with He was only performed very occasionally.

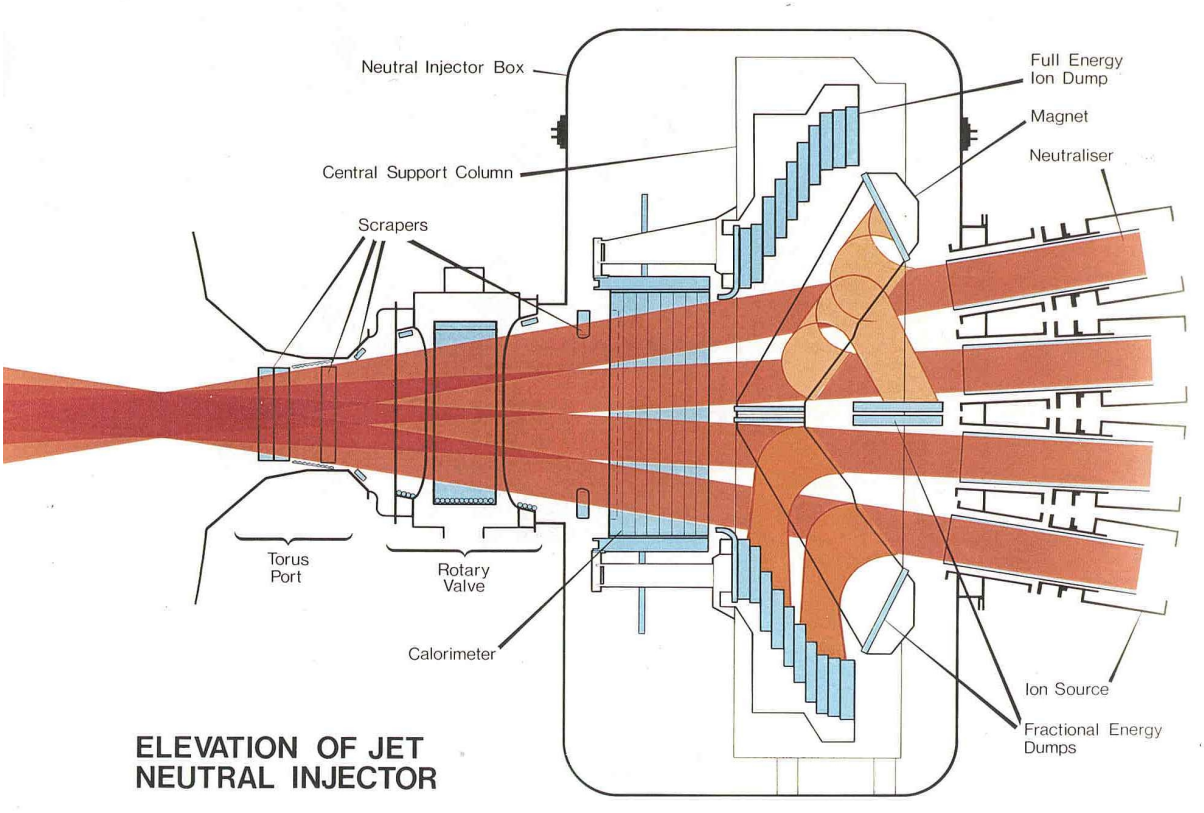

Fig. 2.1: Side view onto the JET neutral beam injector.

Situation at JET

JET has two beam injectors with 8 beam sources each (so-called **P**ositive **I**on **N**eutral **I**njectors or PINIs). The injector installed at octant 4 was operating with 80 kV beam sources rated for approximately 50 A of deuterium beams. The injector at octant 8 was operating with 140 kV beam sources rated for 30 A of extracted deuterium current. The 8 beam sources are arranged in two vertical banks of four sources each. Fig. 2.1 shows a side view onto the JET neutral beam injector.

Situation at ASDEX Upgrade (AUG)

At AUG two injectors with 4 ion sources each, operating at 60 kV (SE injector) or 100 kV (NW injector) extraction voltage are installed.

Pure He beam at AUG (30kV)

At AUG the beam box is equipped with ion-getter pumps, therefore He is not being pumped during the pulse and therefore only short He beam pulses are possible. We did our first HeI beam emission measurements in August 1999 at AUG with ion source Q4 from the SE injector converted to pure He operation. The duration of the He beam pulse was limited to 300 ms and placed at the end of the heating phase, to keep the duct load to a minimum.

After neutralisation the remaining ions are swept out of the beam by a bending magnets. The configuration of the bending magnets in the AUG injector provides the same bending power in all four magnets. In case of one He (4 amu) beam and 3 deuterium beams (2 amu) the extraction voltage of the He beam had to be set to 30 kV - halve the value of the D beams, in order to divert the He beam properly into the ion dump ($U_{He^+} \cdot m_{He^+} = U_{D^+} \cdot m_{D^+}$).

When operating the beam system with D_2 a small fraction of singly charged molecular ions can be left in the beam after the neutraliser. These ions are deflected with $\sqrt{2}$ the bending radius compared to D^+-ions ending up on the so-called “fractional energy dump” designed to take up the power load of these molecular ions. He^+-ions with the same energy as the D_2^+ ions follow the same trajectories.

The measurements of the HeI beam emission at the end of the discharges were “parasitic”. However, the conversion of one ion source to He reduced the available heating power, which could be tolerated at AUG where enough heating power was available. Unfortunately, these first measurements suffered from problems with the spectrometer and an unfavourable beam geometry which made it difficult to separate the Doppler-shifted HeI emission from the unshifted one. However, a first set of HeI beam emission results could be obtained at 30 kV beam energy.

He doping system at JET (octant 4 / 80 kV)

For most of the experimental program at JET all the available heating power is needed. This led to the development of a so-called doped beam in which temporarily a small amount of He gas was added to the deuterium gas fed into the ion source, thus producing a deuterium beam with a helium minority fraction [28]. This procedure has the advantage of producing a fast helium beam fraction without actually reducing the available heating power, and with a negligible He influx to the plasma. The pressure increase in the beam box caused by the unused helium gas was tolerable and the additional power load onto the "fractional energy dump", produced by the residual He atoms in the neutralised beam, was within the specification of this dump.

After tests at the JET test-bed a He doping-system with pre-set timing was installed at the octant 4 injector (80 kV), and first parasitic measurements of HeI beam emission could be made in November 1999.

He doping system at AUG (60 kV)

Following the successful test at JET, a similar He doping system has been installed at AUG at the so-called SE injector. This allowed us to use the so-called "diagnostic PINI" Q3 with a more favourable viewing geometry instead of Q4 which has been used previously for the pure helium beam. Successful measurements with a He doped D-beam at the full beam energy of 60 kV were made in June 2000.

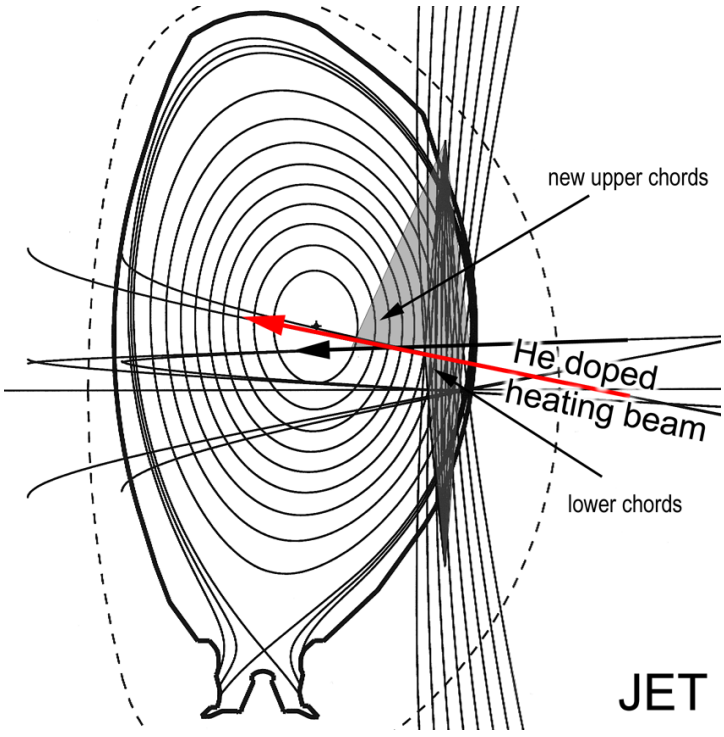

Fig. 2.2: Cross section through the JET plasma showing the beam trajectories and the viewing lines used at the octant 4 injector projected to the cross section.

Improved timing system at JET

During the JET experimental C3 campaign (November 2000) the pre-set pneumatic timing system of the doping system was replaced by a more versatile electronic one. During three dedicated sessions in December 2000 and March 2001 HeI beam emission measurements with doped He/D and pure He beams were performed using either of the two beam injectors installed at octant 4 (~80 kV) and octant 8 (~140 kV).

He beam injection has been performed from one beam source only, either PINI 6 in octant 4 or PINI 7 in octant 8. During these He beam emission experiments the He-PINI (doped or pure) was the only beam source used in the respective injector. By restricting the number of beam sources it was possible to operate the doped deuterium/helium beam for up to 6 seconds without exceeding the limiting pressure in the beam duct. The long pulse duration was required for experiments with plasma sweeping (cf. chapter 2.3). A projection of the beam axes of the octant 4 injector onto the vertical plasma cross section is shown in Fig. 2.2 together with the viewing lines of the KS7 diagnostic.

Experiments with pure He beams could be performed during a dedicated helium campaign, providing measurements with higher He beam currents and therefore higher intensity of the HeI beam emission.

2.2 Spectroscopy

At both experiments for the HeI beam emission measurements the spectroscopic system of the respective charge-exchange diagnostic (CXRS) was used. The CXRS diagnostic monitors visible charge-exchange lines from impurity ions. Derivation of the ion temperature, impurity concentration and collective velocity of the ions is achieved from the width, height and Doppler-shift of the emitted spectral line respectively. In most cases the 529.1 nm line, emitted after electron capture from the fast beam particles (deuterium) into the hydrogen-like C^{V}-state, is used by the CXRS diagnostics.

The observation systems have about 15 viewing lines crossing the beam at different locations, thus covering the plasma from the edge to the core. Both the CX- and the direct beam emission are located at the position of the beam (neglecting plume- and halo-effects). Therefore, the measurements are local and the measured beam emission- and CX-signals are located at the intersection of the viewing lines with the beam (so-called active volumes).

The spectrometers used at both AUG and JET can be set to a wide range of wavelengths which covers the visible n = 3 → 2 and n = 4 → 2 transitions of atomic helium (cf. Fig. 1.2).

HeI spectrum

A typical HeI beam emission (2^3P-3^3D / 587.6 nm) spectrum (left plot) is shown in Fig 2.3 together with a D_α beam emission spectrum (right plot) measured with the same diagnostic (JET/KS5). In order to be able to compare the peak widths the HeI beam emission peak (red shaded) is reproduced in the right hand plot (not at its correct wavelength).

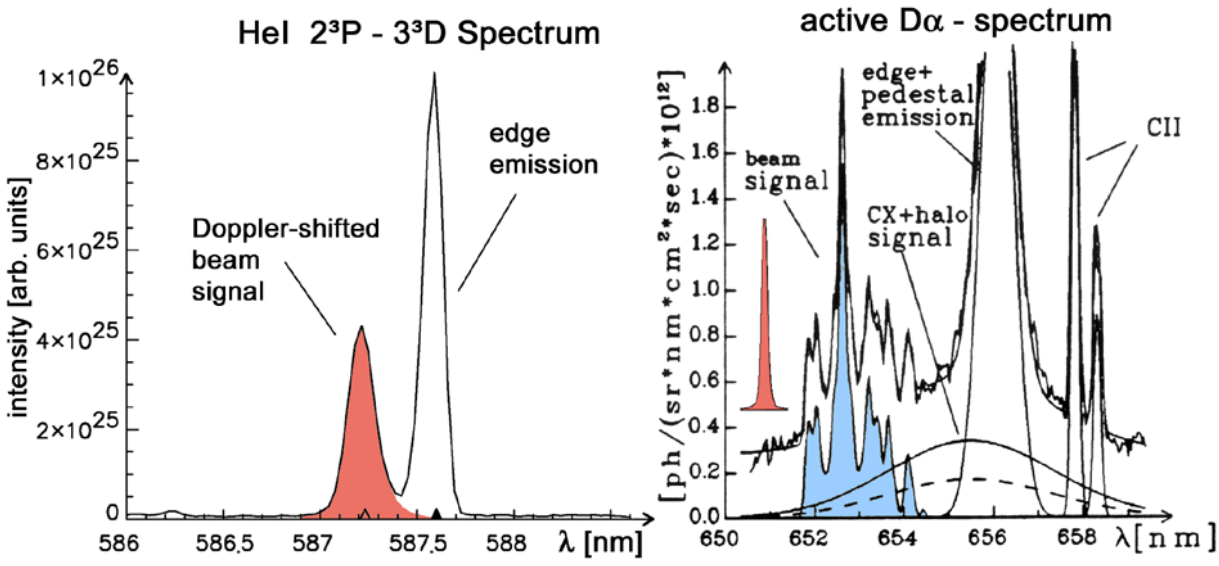

Fig. 2.3: Comparison of the 2^3P-3^3D (587.6 nm) HeI beam emission spectrum (left graph) with the D_α-spectrum (right graph). The shaded peaks (He red and D blue) results from the respective excited beam particles.

For the HeI spectrum the spectrometer was used with a relatively wide opening of the entrance slit, in order to get high signal intensities. This leads to an instrumental function of the spectrometer with a typical width of

0.1 ... 0.2 nm (FWHM). Therefore, the real width of the peaks in Fig 2.3 are significantly smaller. The highest peak of the spectrum is the unshifted passive plasma emission from the edge. The Doppler-shifted emission from the excited beam particles (He red / D blue) is marked by shading.

Obviously the D_α beam emission spectrum is much more complex than that from the HeI emission, due to four facts:

1) Helium in contrast to deuterium is a minority species of the plasma and therefore the charge-exchange halo of the beam is much weaker.
2) The linear motional stark splitting of the D_α is much larger than the quadratic effect in the case of He, which is below the resolution of the spectrometer.
3) The deuterium beam, in contrast to helium, is composed of three components with 100%, 50% and 33% of the beam energy respectively.
4) The passive HeI emission appears within a narrow peak and therefore well separated from the beam emission, even for relatively small Doppler-shifts. Helium is a common impurity in fusion devices, because it is frequently used for glow discharge cleaning of the vacuum vessel. However, significant equilibrium fraction of atomic He involves temperatures below 2 eV. HeI emission from the plasma is therefore limited to the cold plasma edge.

This simplicity of the HeI spectrum is a big advantage as the spectral analysis can easily be automated and evaluated with high accuracy.

Doppler-shift of beam emission

The beam energies used for our beam emission measurements are in the range from 30 keV to 140 keV, corresponding to particle speeds in the range of $(1.2 – 2.6)\ 10^6$ m/s. The resulting Doppler-shift of the emitted light is large enough for separating the beam emission peak from passive HeI plasma emission, provided the angle between beam axis and viewing line is not close to 90°. E.g. the beam emission of the 587.6 nm line (2^3P-3^3D) cannot be separated from passive emission for observation angles in the range of 90±5°.

2.2.1 Spectroscopic system at AUG (CER diagnostics)

The CER diagnostics collects light from the plasma via a mirror mounted in a port of vessel segment 13. A lens system focuses this light onto a plate holding optical fibres. These fibres define the viewing-lines fanning out horizontally from the optical head to the beam from the ion source Q3 (and Q4) of the SE injector. Fig. 2.4 shows a plan view of the set-up.

The collected light is transmitted via optical fibres across the biological shield to a Czerny-Turner spectrometer (type BM 100). The fibres are arranged in a single vertical line array in front of an adjustable entrance slit. A programmable CCD Camera is operated with typical exposure times of 20 – 50 ms, and the data read-out time is about 15 ms. The used

2400 lines/mm grating leads to a dispersion of 0.09 Å/pixel and can operate in the range 300-680 nm. Wavelength settings above 680 nm are prohibited by the control software, although the spectrometer could be operated at higher wavelengths. Therefore the 728 nm (2^1P-3^1S) and the 707 nm (2^3P-3^3S) HeI emission lines could not be measured at AUG.

Doppler-shift

For the measurements at AUG we used the ion sources Q3 and Q4. When using the source Q4 the observation angle was too close to 90° for many viewing lines (see above). The situation is better when using the ion source Q3 (see Fig. 2.4).

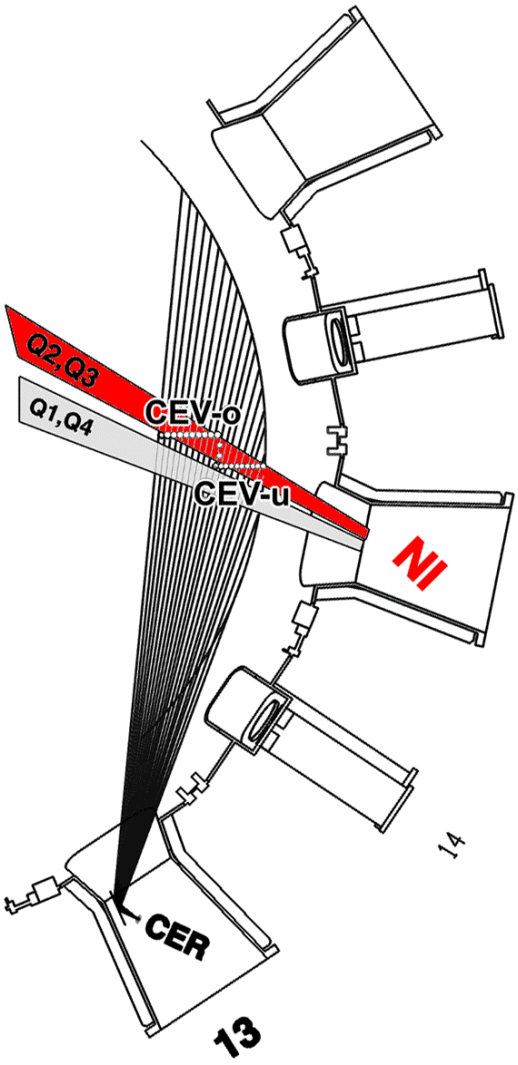

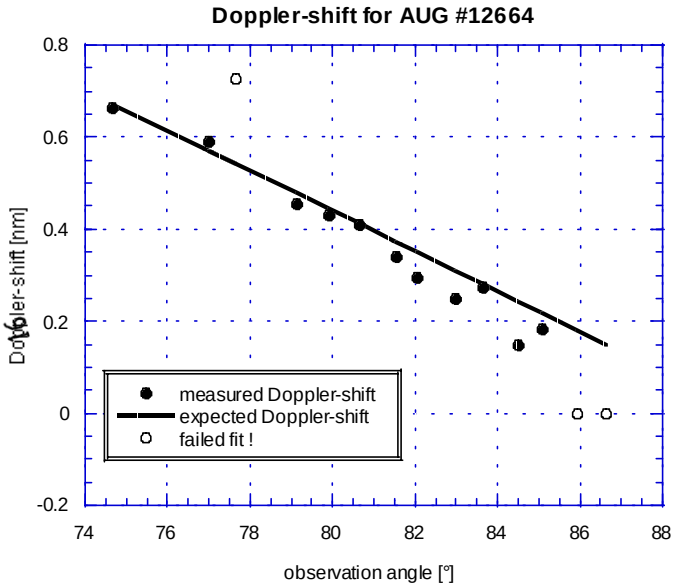

Fig. 2.5: Expected (solid line) and measured (dots) Doppler-shift of 667.8 nm (2^1P-3^1D) HeI beam emission observed during AUG pulse #12644. The open dots are used for tracks, where the fit procedure failed.

Fig. 2.4: Plan view of a segment of AUG. One can see the fan of viewing lines crossing the beams from ion source Q3 and Q4. The beam from Q3 can be operated as a doped He/D beam (marked red).

As mentioned above, for our first measurements at AUG one ion source was converted to He operation. During the CX-diagnostics measurements it was necessary to operate Q3 in D. Therefore Q4 had to be used for the generation of the pure He beam. In Fig 2.5 the expected (solid line) and measured (dots) Doppler-shift of the 667.8 nm (2^1P-3^1D) HeI beam emission observed during AUG pulse #12644 is shown. Because the Doppler-shift is too small for observation angles above 85° the beam emission could not be distinguished

from the passive plasma emission, and the curve fit failed (open dots). The beam emission peak measured with an observation angle of 77° was disturbed by a Si impurity line.

For the He doping system the ion source Q3 could be used, yielding better peak separation due to higher Doppler-shift.

2.2.2 Spectroscopic system at JET (KS4,5,7 diagnostics)

For the experiments at JET two different CX-diagnostics have been used, depending on the injector used for generating the He beam. For the 80 kV injector at octant 4 the so-called KS7 diagnostics and for the 140 kV injector at octant 8 the so-called KS4/5 diagnostics was used for observing the beam emission.

KS7 system

The KS7 diagnostics is mainly used for measuring ion temperature at the plasma edge via C-charge-exchange [33]. Two so-called optical heads are situated in vertical ports above and below the beams of octant 4 (see Fig 2.6). The original design of the optical head [34], consisting of a lens-system and a fibre plate, was designed to provide a fan of viewing-lines covering the plasma edge with good spatial resolution (> 20 mm).

The optical head of the upper port has been redesigned to cover the full range of the plasma from the edge to the core with a higher light throughput but lower spatial resolution (> 60 mm). These viewing lines are used for measuring the collective velocity of the plasma (plasma rotation) from the Doppler-shift of the CX-signal.

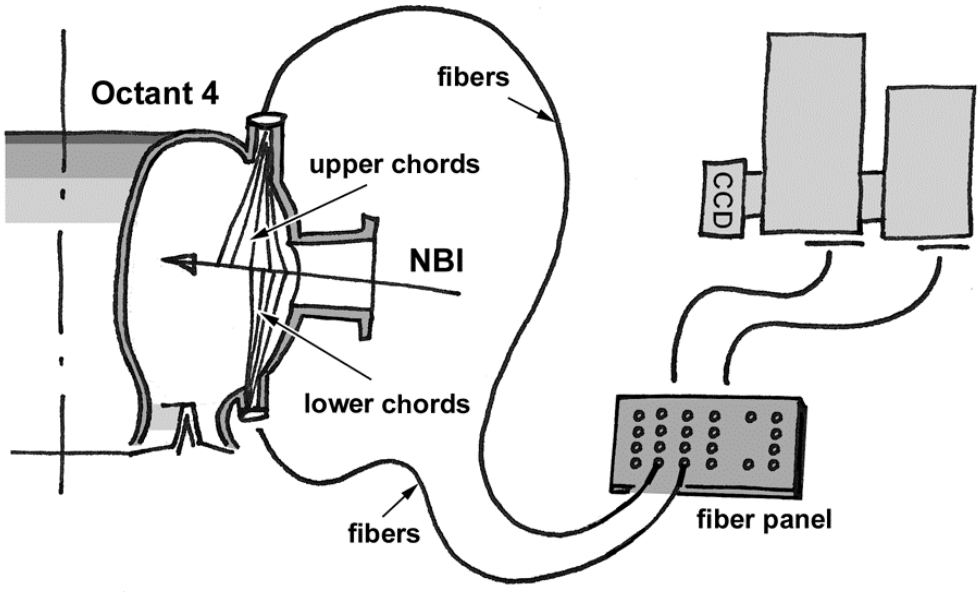

Fig. 2.6: A sketch of the KS7 diagnostic with its main components optical head, fibre panel and the two spectrometers.

The light collected by the optical head is transmitted through optical fibres to the spectrometer situated outside the biological shield. A special feature of the KS7 system is a fibre panel, where a subset of fibres can be easily selected and plugged into the panel.

In normal operation of the KS7 diagnostics two Cerny-Turner spectrometers are used in series (in the following called "standard mode" – see Fig 2.7). The first spectrometer acts as a band-bass filter and the second one as the spectral analyser. The band-pass spectrometer is used to fit spectra from 4 fibres onto a row of the CCD sensor without cross-talk, which makes it possible to image an array of 4x4 fibres simultaneously.

The band-pass spectrometer is a McPherson model 207 of Cerny-Turner design with a focal length of 0.67 m and a 600 lines/mm grating. This kind of spectrometer suffers from anamorphic magnification. In order to get an undistorted image on the CCD sensor, the entrance slit is shaped to compensate for this effect. This shape is calculated for the design central wavelength (λ = 529.1 nm) by ray tracing through the spectrometer.

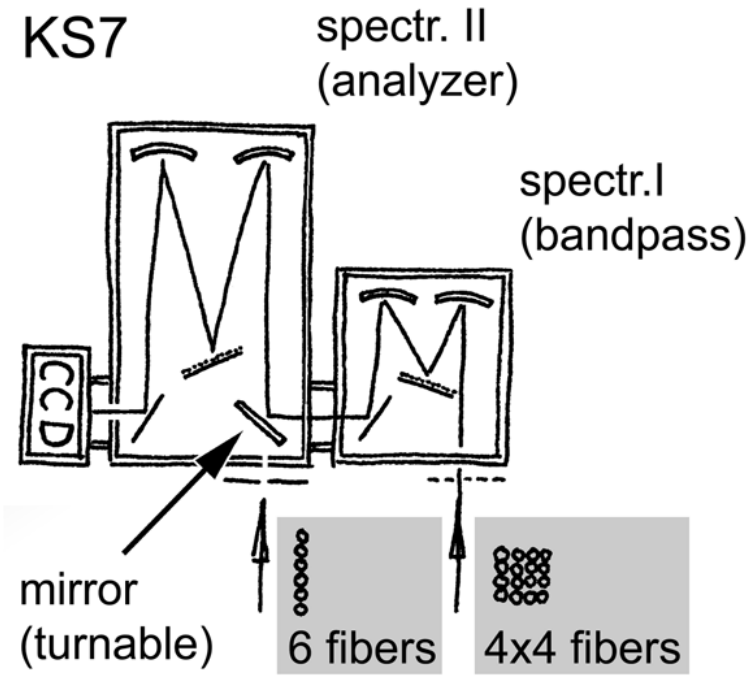

Fig. 2.7: Schematic view of the KS7 spectrometer with two spectrometers in series ("standard mode" of operation).

The analysing spectrometer, a McPherson model 209 Cerny-Turner spectrometer with a focal length of 1.33 m, has been fitted with a 2400 lines/mm ruled grating.

It is possible to bypass the band-pass spectrometer, by changing the mirror position (see Fig 2.7) and using another entrance slit (single slit). In this mode the number of observable fibres has to be reduced from 16 to only 6 fibres. This yields a 4 times bigger wavelength range, and there is no distortion of the image (in the following called "6 fibres-mode").

During the 1999 campaign several parasitic measurements with the KS7 system have been performed in either the standard- or in the 6-fibre-mode. It turned out that in the standard setup with 16 fibres the bandwidth was too narrow for some of the fibres and could thus not cover the range of the unshifted and the Doppler-shifted peak. Although it was in principle possible to correct the data subsequently, such a correction introduced additional intolerable errors.

Therefore, during the campaigns in 2000 and 2001 KS7 was only used in the 6-fibres setup. To compensate for the smaller number of fibres, a sweep experiment was introduced (see chapter 2.3).

KS7 provides a large number of lines-of-sights, which can be changed easily on a shot-by-shot bases. However, an absolute calibration of the system has so far only been performed for one set of fibres.

These fibres where chosen according to the following requirements:

- Doppler-shift sufficiently large to separate beam emission from the passive emission.
- Avoiding viewing lines for which the Doppler-shifted He emission is masked by emission from impurity lines.
- Distance between neighbouring active volumes (intersection of line-of-sights with the beam) small enough for "overlapping calibration" (< 100 mm).

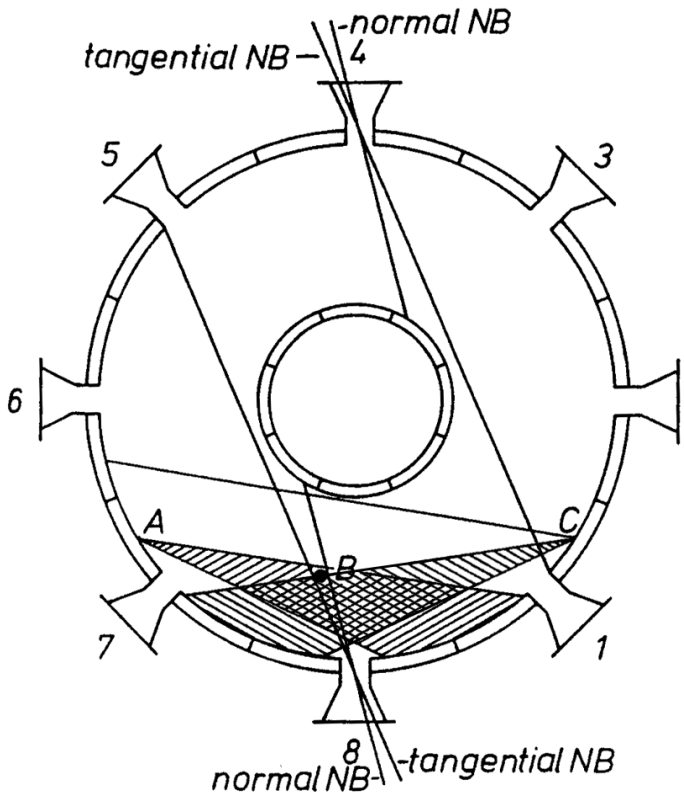

Fig. 2.8: Plan view of the JET vessel showing the neutral beam trajectories and the fans of viewing lines (hatched areas). Position A (oct 7) and C (oct 1) are the locations of the optical heads of the two periscopes. B marks the vertical port of the single viewing line of KS4.

KS5 system

The KS5 charge exchange system uses fibres coming from two periscopes (octant 1 and 7) looking at the beams of the octant 8 injector. The fans of lines-of-sight are shown in Fig. 2.8 together with the beam trajectories.

The optical head with the adjustable mirror is shown in Fig. 2.9. The fibres form the two periscopes are distributed to three spectrometers (KS5a/b/c), making simultaneous measurement for different wave-lengths possible. Fig 2.10 shows a sketch of the KS4/5 system.

All three spectrometers are of Czerny-Turner design and use a subset of up to 12 fibres and a single entrance slit. The detectors are PC-controlled back-illuminated CCD sensors.

Due to coating of the plasma facing optical components and ageing of the fibres the light throughput has decreased by different amount from fibre to fibre, and the signal

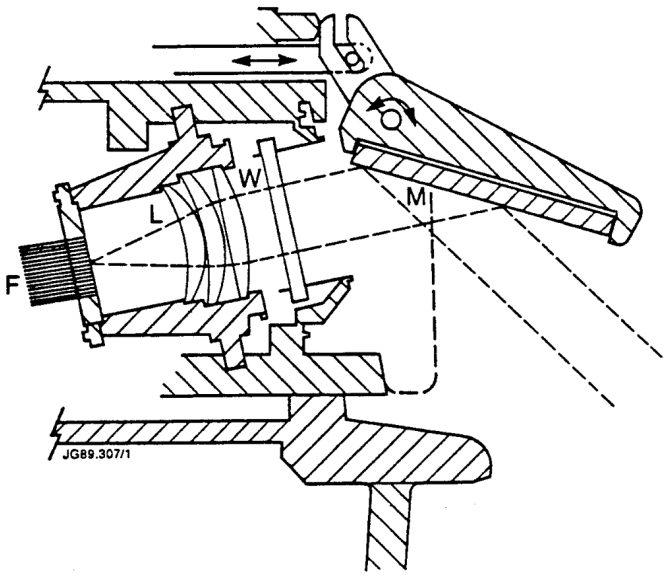

Fig. 2.9: Sketch of the optical head of the periscopes, consisting of a stacked fibre bundle (F), lens system (L), vacuum window (W) and fold-back mirror (M).

intensities were quite different for the various instruments. Because KS5a provided the highest signal intensities the measurements have been performed mainly with this spectrometer.

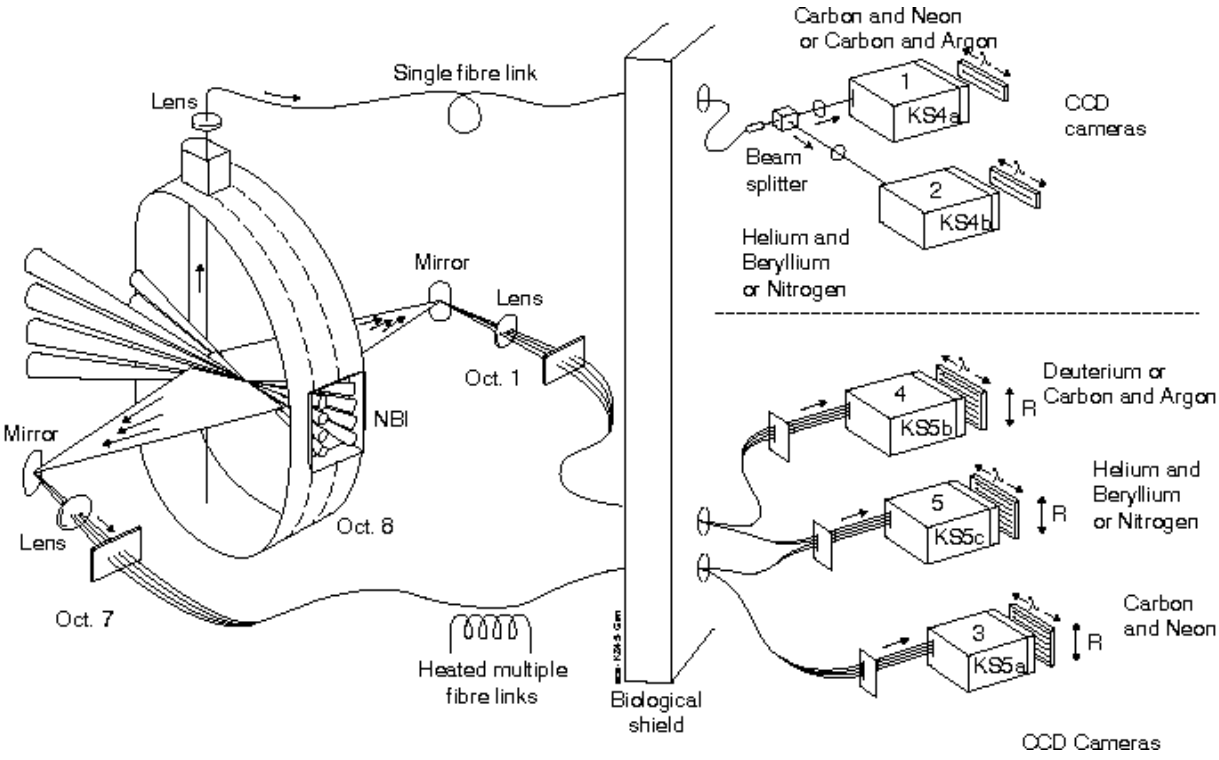

Fig. 2.10: Viewing lines of the KS5 spectrometer used for the 140 kV beam from the octant 8 injector.

The viewing lines from KS5a are crossing the beams from both ion sources PINI 6 and 7. In Fig. 2.11 the estimated Doppler-shifts for the 587.6 nm (2^3P-3^3D) beam emission for a 140 keV He beam (PINI 6 and 7) are plotted for the KS5a viewing lines. When installing the He doping system at PINI 7, the Doppler-shift was sufficient for all tracks. The shaded areas indicate unfavourable values of the Doppler-shift, overlapping the beam emission in the 587.6 nm spectrum with either passive HeI emission or an impurity line.

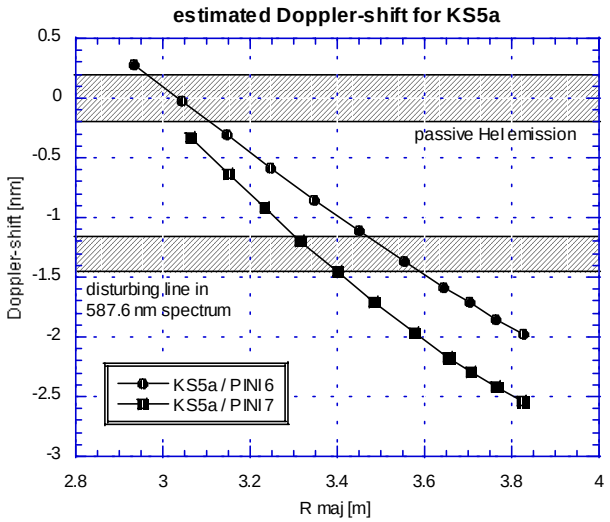

Fig. 2.11: Estimated Doppler-shifts for the KS5a viewing lines for the 587.6 nm (2^3P-3^3D) beam emission coming from a 140keV He beam (PINI 6 and PINI 7).

2.3 Plasma sweep experiments

During the first HeI beam emission measurements at JET by using KS7 it turned out that this diagnostics could only be used in its 6-fibres setup (see chapter 2.2.2) with a corresponding loss in radial resolution. To recover in radial resolution the sweep experiment was introduced.

2.3.1 Radially swept high clearance X point L-mode plasma

This type of plasma has been used previously for measuring the edge density with an interferometer channel, which on its own can only measure the line integrated density. By sweeping the plasma in radial direction the line integrated density varies with time and the local density can be extracted by means of an Abel inversion. Fig. 2.12 shows that the edge density profile measured in this way is well reproducible, which is confirmed by edge LIDAR measurements derived from Thomson scattering.

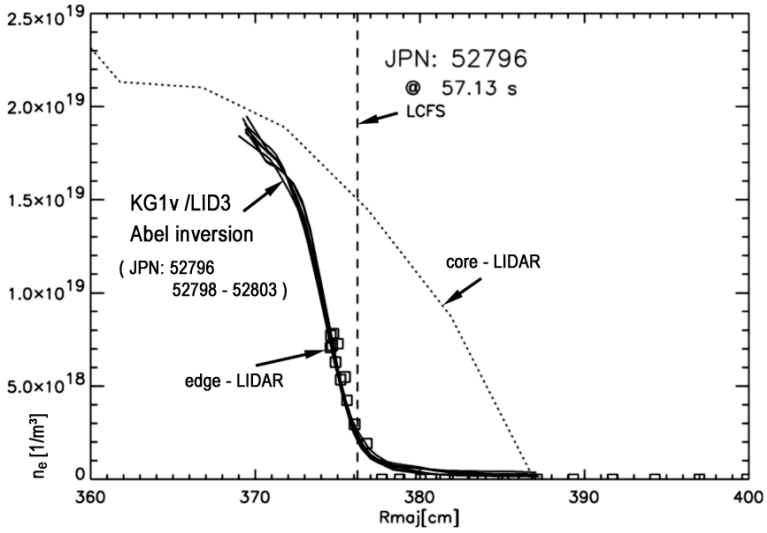

Fig. 2.12: Density profiles for a series of identical L-mode sweep pulses derived by the Abel-inversion of edge-interferometer data during sweeping

For this plasma sweeping a so-called L-mode plasma has been used in order to avoid the noise introduced in H-mode plasmas by ELMs. One consequence of using a L-mode plasma was that the heating power had to be kept below the H-mode threshold. Plasma temperature- and density profiles of the swept L-mode plasma measured with the standard diagnostics of JET are shown in Fig. 2.13. The abbreviations of the used diagnostics are explained in Tab. I.

KK1	ECE Michelson Interferometer	T_e profile	
KK3	ECE Heterodyne Radiometer	T_e	
LIDR	LIDAR Thomson scattering	T_e	n_e
KE9D	edge LIDAR	edge T_e	edge n_e
KY63	Li beam		edge n_e

Table I: Abbreviations for the standard electron density- and -temperature diagnostics at JET.

The measured electron densities and -temperatures are mapped onto the beam axis, and a subsequent fit gives smooth profiles used for our later model calculations (for details see chapter 3.2).

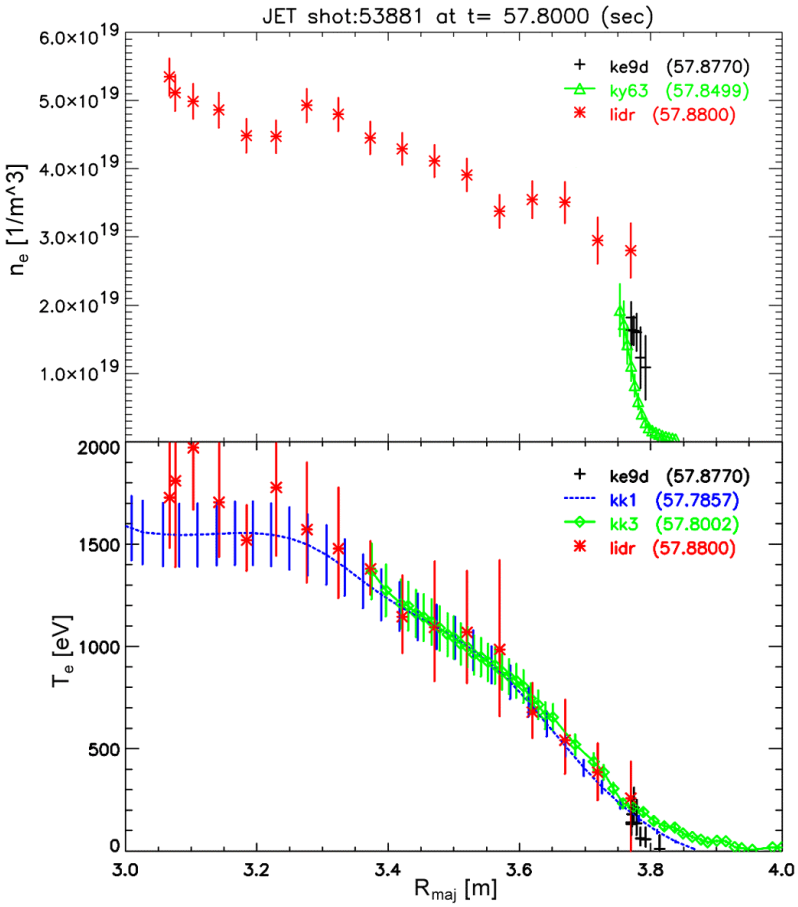

Fig. 2.13: Temperature- and density profiles of a L-mode plasma used for the sweep experiments, as measured with the standard diagnostics.

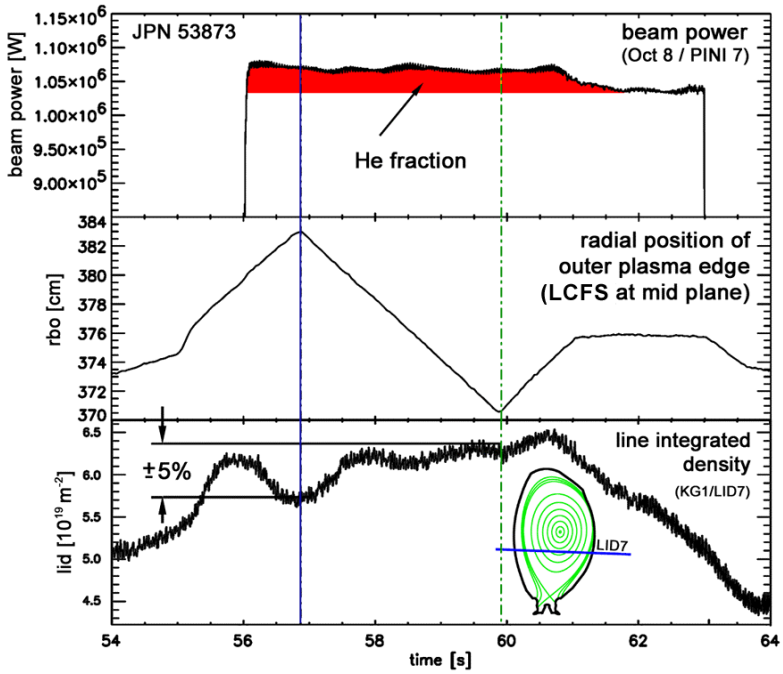

Fig. 2.14: Injected beam power (top), location of the LCFS in the mid plane (middle) and plasma density. The duration of He doping is visible as increase in the injected power and marked by shading.

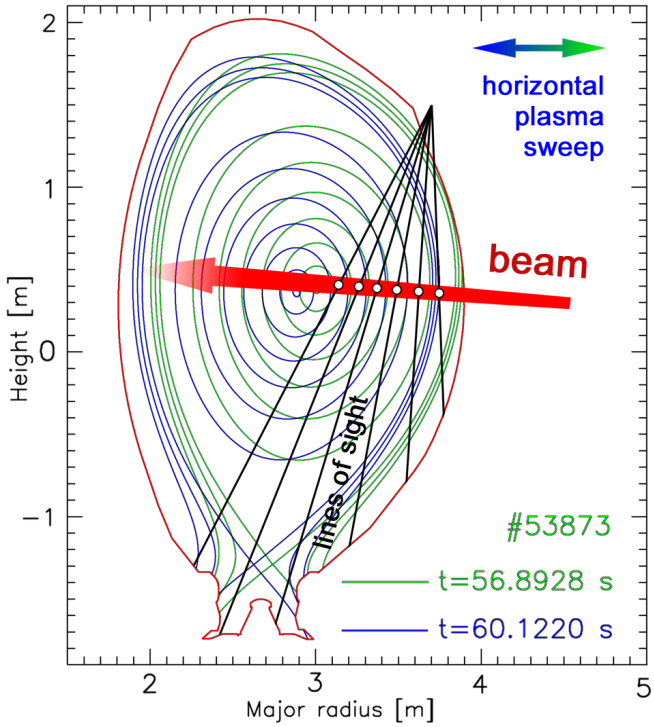

Fig. 2.15: Flux surfaces from EFIT for the extreme plasma positions of the radial sweep.

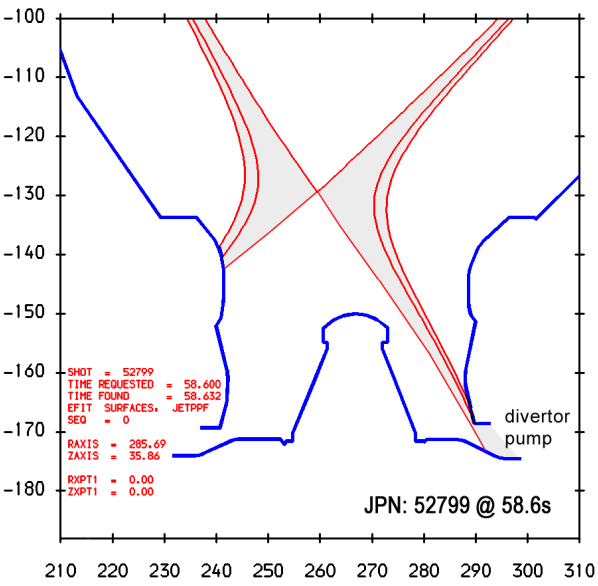

Fig. 2.16: Strike point location for increased pumping.

The plasma was swept radially by 120 mm with a ramp rate of 40 mm/s. The location of the last closed flux surface (LCFS) in the mid-plane is shown in Fig. 2.14 together with the injected beam power and the line-integrated density.

The plasma shape was made very slim, in order to avoid interaction between vessel wall and plasma at the extremes of the sweeps. The two extreme positions of the flux surfaces are shown in Fig. 2.15.

pulse	D_2/CD_4	Z_{eff}	$<n_e \cdot dl>$
53872	CD_4	2.1	8.9
53873	D_2	1.7	11.8
53874	CD_4	2.1	9.3
53875	D_2	1.7	10.5
53876	D_2	1.8	10.0
53877	CD_4	2.1	10.0
53878	CD_4	2.1	10.0
53879	D_2	1.9	10.0
53880	D_2	1.9	10.0
53881	D_2	1.9	10.0
53882	D_2	1.9	10.0

Table III: Line-average density in $10^{19}/m^2$ and average impurity level Z_{eff} for the pulses of our second measuring campaign.

line averaged density	7-10 $10^{19} m^{-3}$
central el. temperature	1.5 - 2 keV
toroidal field	2.4 Tesla
Plasma current	2.5 MA
add. heating	3 MW

Table II: Main plasma parameters of the JET discharge used for the He beam emission experiments.

One problem with the first plasma sweep pulses was caused by dropping of the plasma density when the strike point passed over the gap between horizontal and vertical target in the divertor (see Fig. 2.16). This drop in density can be explained by a accordingly stronger pumping. The plasma density variation during the sweep could be kept below 5% by limiting the sweep to a range where the outer strike-point stayed on the vertical target tiles.

The measurements were performed with a series of nominally identical pulses. However, the Z_{eff} was varied by injecting either deuterium or CD_4 into the plasma. Table II shows the main plasma parameters of the discharge and table III shows the reproducibility of the plasma density when Z_{eff} was varied.

2.3.2 Cross-calibration of the spectrometer channels using plasma sweep data

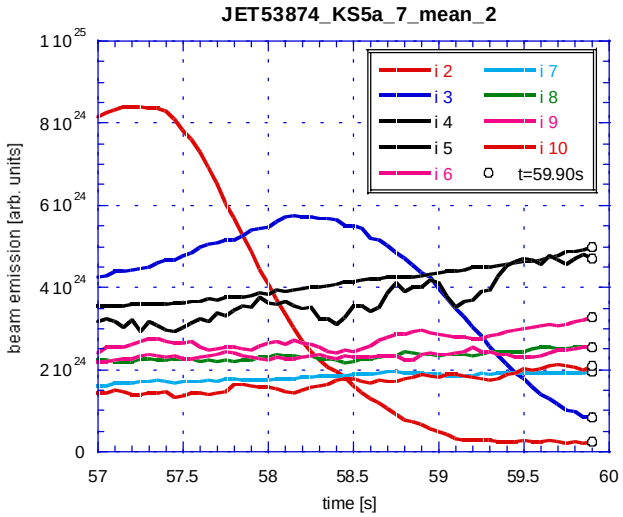

Fig. 2.17: Photon flux of the HeI beam emission (667.8 nm) measured with the KS5a diagnostic during a horizontal plasma sweep (JPN 53874). Different colours for different lines-of-sight.

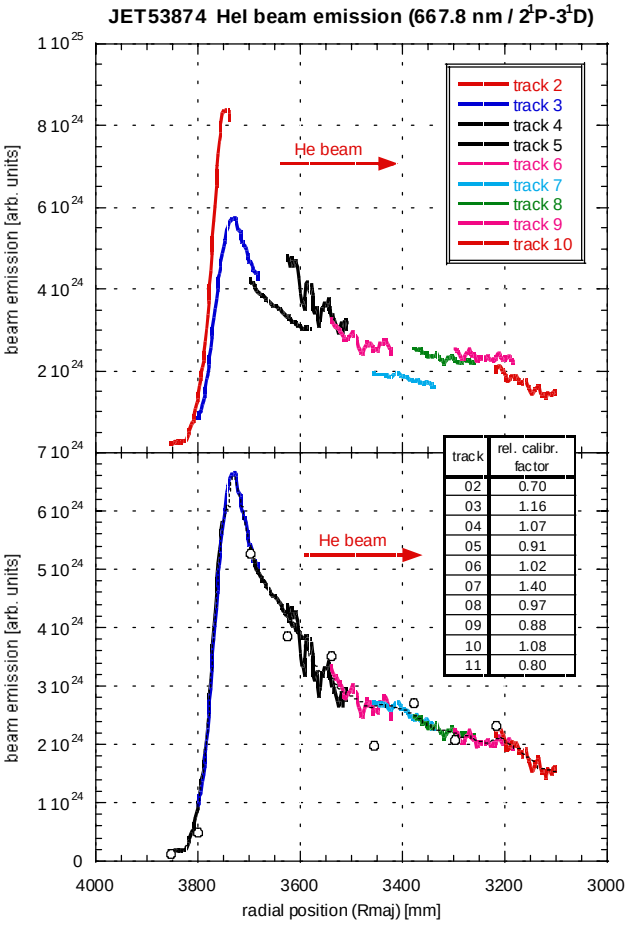

Fig. 2.18: Upper graph: Data shown in Fig. 2.17 mapped to respective major radius at t= 58 s. Lower graph: Same data after "overlap"-calibration.

As the plasma sweep was wide enough to overlap neighbouring viewing lines, it was possible to check the calibration of the viewing lines and to cross calibrate them where required. Fig. 2.17 shows the photon flux of the HeI beam emission (667.8 nm) measured with the KS5a system at different lines-of-sight (different colours) plotted vs. time. Over the time span displayed (57-60 s) the plasma has been moved horizontally by 120 mm across the viewing lines.

The upper graph of Fig 2.18 shows the same data mapped to the respective major radius at t = 58 s. One can clearly see that the different profile sections match very well in shape, but the absolute intensities differ from each other. To overcome these inconsistencies an additional calibration factor (overlap-factor) has been introduced for each track. These factors were derived by matching overlapping areas of adjacent channels by means of a least-squares-procedure.

The individual calibration factors are restrained by the condition that the average over all tracks is unity. This leads to unambiguous values and keeps the influence on the absolute calibration of the data small.

The result of the "overlap-calibration" of the data from Fig. 2.17 is shown in the lower graph of Fig. 2.18.

The observation that the individual viewing lines require individual calibration factors to yield a smooth profile indicates that the calibration of the spectrometer was not perfect. From the standard edge ion temperature measurements (KS7 diagnostic), emission profiles from the C^{VI}-CX line (529.1 nm) are available for very different sweep pulses (L-mode / H-mode, different sweep-ranges, ...). The overlap-factors derived for these pulses support the assumption of an incorrect calibration. Table IV shows the mean values of the derived relative calibration factors for 5 neighbouring tracks. The small scatter (±) in the overlap-factors for these quite different plasmas shows that the difference in measured intensity is indeed caused by calibration errors for the different lines-of-sight (fibre id / chord number). In the case of the calibration factors in table IV the procedure was started at the plasma core and proceeded stepwise towards the edge. This implies an accumulation of the error from the centre towards the edge.

R maj	fibre id	lower chord	ol-factor	+/-
3.64	10	28	1.00	0
3.66	9	25	0.66	0.01
3.69	8	22	0.86	0.025
3.71	7	19	3.19	0.07
3.74	6	16	1.24	0.155

Tab. IV: "overlap"-factors (ol-factor) for 5 lines-of-sight (lower chords / fibre id) of the KS7 system derived from a least-square-fit of the overlapping C-CX emission profile.

This in-situ cross calibration was performed for each pulse. In Fig. 2.19 the introduced "overlap-calibration-factors" are shown for four successive pulses with the KS5a spectrometer at a fixed wavelength setting (667.8 nm).

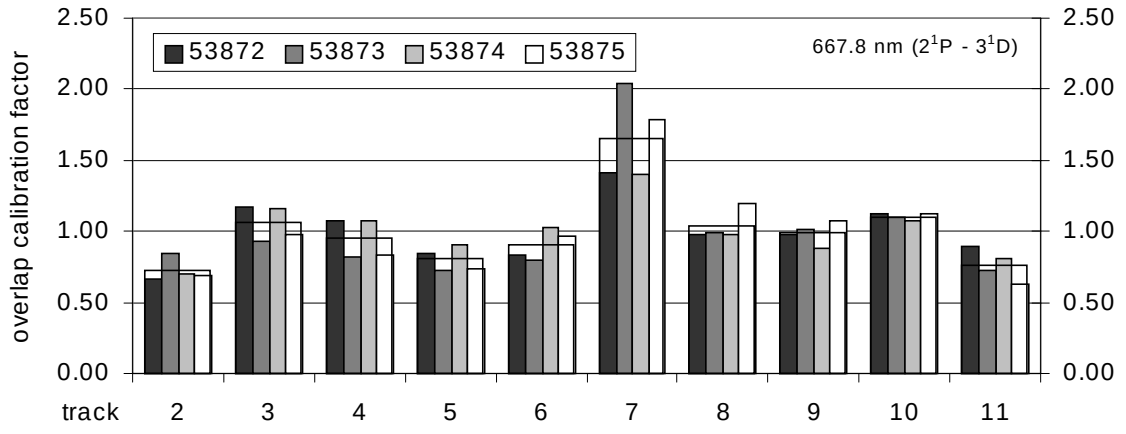

Fig. 2.19: Overlap-calibration-factors for four successive pulses with the spectrometer set to 667.8 nm.

The accuracy and reliability of the method is demonstrated in Fig. 2.20 showing profiles from two repetitive plasma pulses, which were taken with different spectrometers looking at different beams. The profiles match very well after having been shifted against each other by 20 mm. This could

either be due to a mapping error or a consequence of the sweeping (mapping based on different time slices). The model calculation confirms that the attenuation of the 2^3S state is essentially the same for a 75 keV and a 135 keV beam (see Fig. 2.21). For details of the modelling see chapter 4.2. The good match between the two profiles which are taken with different spectroscopic systems using two different He beams is therefore a confirmation of the accuracy of the measurement.

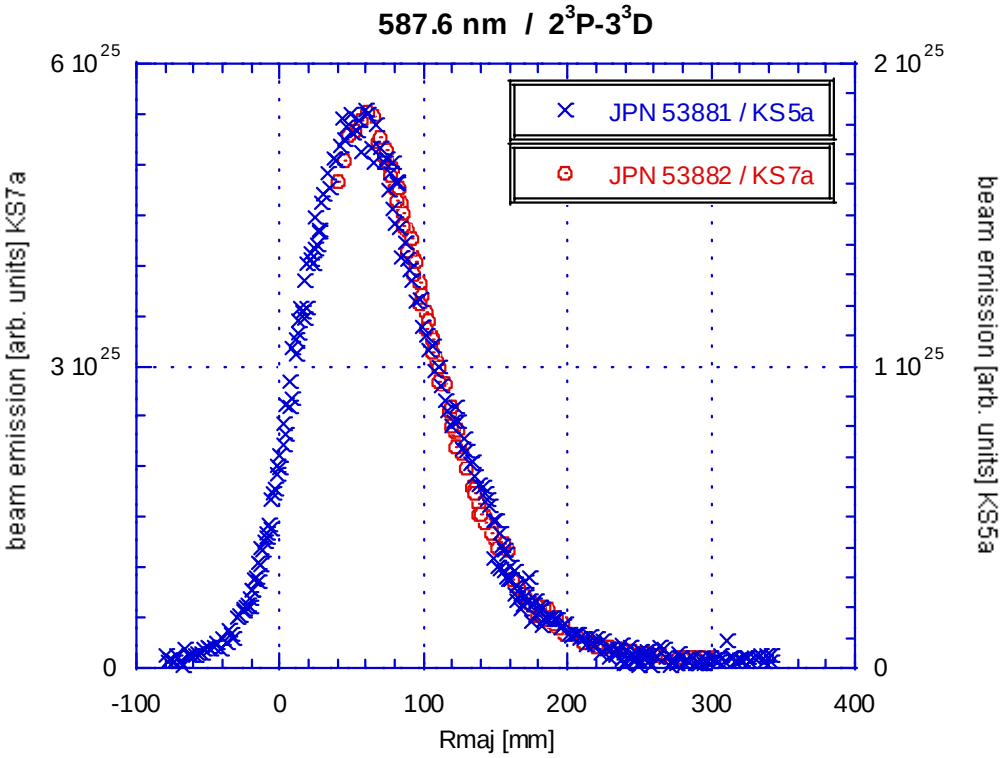

Fig. 2.20: Profile of the emission of a HeI triplet line measured with the spectrometer KS7 looking at a 75 kV beam and with KS5a looking at a 135 kV beam, for two repetitive pulses. The profile measured with KS7 was shifted radially by –20 mm against the other profile.

Another effect of using plasma sweeping is a large noise level of the beam emission data, which manifests itself mainly in sections with small gradients (Fig. 2.22). The integration time of the spectrometer was set to 50 ms or 100 ms to keep the plasma movement during the exposure as small as possible (2 or 4 mm, resp.).

The large scatter was considerably reduced by smoothing over 10 frames, which corresponds to a plasma range of 20 mm and is still small compared to the spatial resolution of the spectroscopic system.

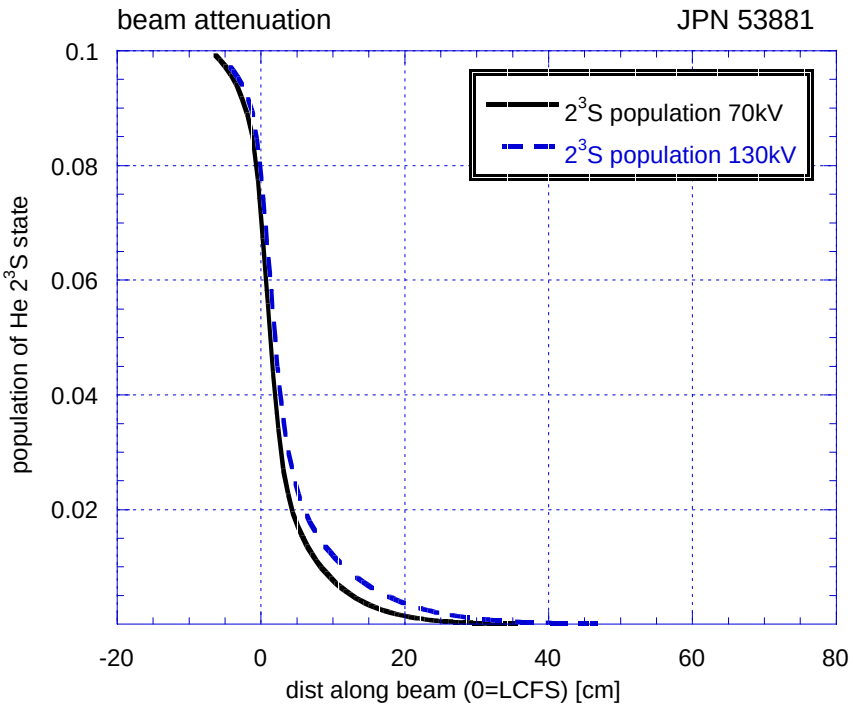

Fig. 2.21: Modelled beam attenuation of the 2^3S level for two different beam energies.

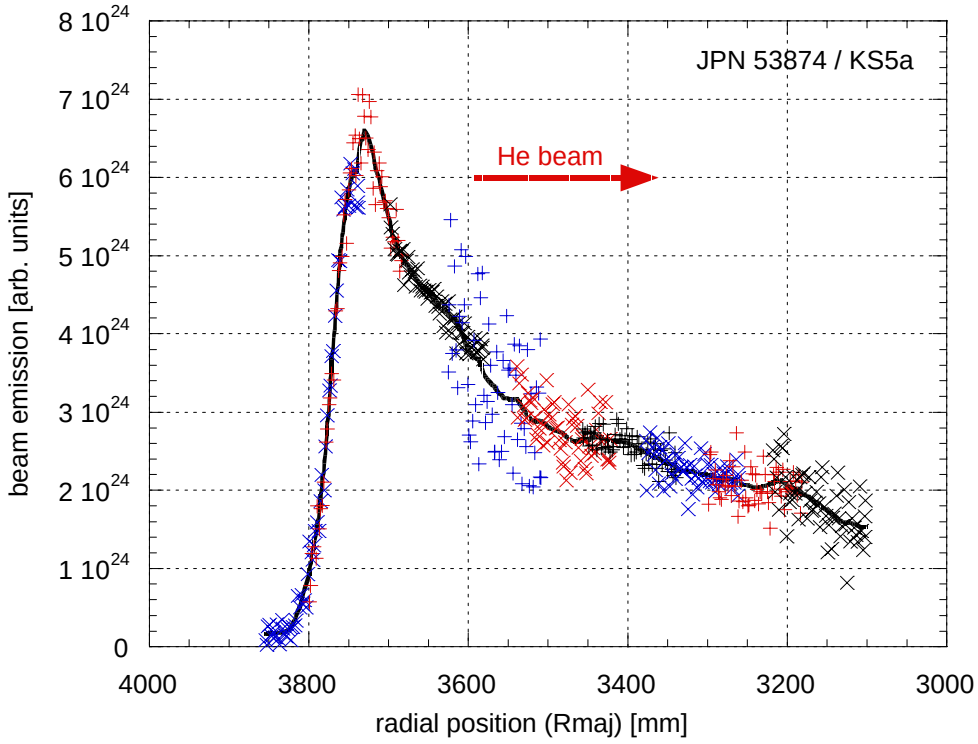

Fig. 2.22: Emission profile for the HeI singlet line 667.8 nm (2^1P-3^1D). The symbols are data (spaced 2 mm) resulting from the fit of single frames (50 ms exposure time). The solid line gives an average over 10 data points, corresponding a distance of 20 mm.